Photopyroelectric ac calorimetric study of the nematic–smectic-*A* phase-transition line in binary liquid crystal mixtures with injected smectic-*A* phases

J. Caerels, C. Glorieux, and J. Thoen*
Laboratorium voor Akoestiek en Thermische Fysica, Department Natuurkunde, Katholieke Universiteit Leuven, Celestijnenlaan 200 D, 3001 Leuven, Belgium

(Received 17 October 2001; published 8 February 2002)

Using a recently developed photopyroelectric ac calorimetric technique we investigate two binary liquid crystal mixtures with so-called injected smectic-*A* phases. Characteristic of these systems is the occurrence of nematic-to-smectic-*A* transition lines in the phase diagram of mixtures of pure compounds having only a nematic phase. The two binary systems are pentylcyanobiphenyl with either 4-*n*-propylcyclohexyl-carboxylate or 4-*n*-pentylphenyl 4′-*n*-pentyloxybenzoate. Both these systems have domelike smectic-*A* ranges with narrow nematic ranges at the top. Near the top the *N*-Sm*A* transitions are of first order and are crossing over to second order at a tricritical point on either side of the top with the increasing width of the nematic range. The obtained critical exponents are almost completely Fisher renormalized because of the strong concentration dependence of the nematic-to-smectic-*A* transition temperatures.

DOI: 10.1103/PhysRevE.65.031704 PACS number(s): 64.70.Md, 65.20.+w

I. INTRODUCTION

In the past calorimetric studies have contributed substantially to better understanding of phase transitions in general and of phase transitions in liquid crystals in particular. Although differential scanning calorimetry (DSC) plays an important role as general characterization tool, detailed thermal phase-transition information is, however, mainly obtained with high-resolution adiabatic and ac calorimetric techniques [1–3].

Although, unlike adiabatic scanning calorimetry, ac calorimetry does not allow one to determine latent heats and distinguish between first- and second-order phase transitions, the method allows for a detailed investigation of pretransitional specific heat capacity C_p anomalies and to determine critical exponents. Indeed, our present knowledge of detailed behavior of C_p near phase transitions in liquid crystals is to a large extend obtained from high-resolution ac calorimetry.

The nematic–smectic-*A* (*N*-Sm*A*) phase transition has undoubtedly been the most extensively investigated of all liquid crystal phase transitions. In the nematic phase, rodlike molecules align with their long axes parallel, resulting in orientational order on a microscopic scale parallel to the director. In the Sm*A* phase in addition to this, the system develops a one-dimensional density wave resulting in one-dimensional position ordering (layering). The smectic wave vector of this density wave is parallel to the nematic director. The basic aspects of the *N*-Sm*A* phase-transition behavior was formulated by de Gennes in terms of the close analogy with the normal-superconducting phase transition in metals and in terms of a Landau mean field energy expression, which included a coupling between the amplitude of the Sm*A* density wave and the nematic order parameter [4,5]. Depending on the strength of the coupling between these two order parameters, the *N*-Sm*A* transition can either be of first order or second order. For narrow nematic ranges (between the isotropic and the smectic-*A* phase), the transition is first order becoming second order via a tricritical point for wider nematic ranges. In order to make further progress beyond the mean field approach, fluctuations have to be properly taken into account. The fact that in reality the smectic-*A* order parameter has two components led de Gennes [4] and McMillan [6] to conclude that the *N*-Sm*A* transitions should belong to the *XY* universality class for an order parameter coupling-free situation. Most further theoretical studies and attempts to calculate critical exponents beyond the mean field have been based on a free-energy functional introduced by de Gennes [4], which is formally very similar to the Ginzberg-Landau free-energy functional for superconduction.

Although there have been several theoretical efforts, at the present time there exists no clear theoretical consensus about the exact nature of the critical behavior of the de Gennes model and about the validity of the predictions for the *N*-Sm*A* transition from the superconducting analog [7]. Important differences are the absence of true-long-range smectic order in three dimensions [8] and the presence of the splay elastic term in the de Gennes free-energy functional. These complications make it very difficult to properly take into account thermal fluctuation effects to arrive at the modified critical exponents beyond mean field theory. According to a prediction made by Halperin, Lubensky, and Ma [9] in 1974, fluctuations not only change the critical exponents, but may drive a second-order phase transition to a first-order one when two order parameters are simultaneously present and interact with each other. They predicted this to be the case for the *N*-Sm*A* transition in liquid crystals and for the normal-superconductor transition for type-1 superconductors. In addition to fluctuations in the nematic order parameter *S* (as in the de Gennes–McMillan approach) they also considered director fluctuations beyond mean field. This extension was sufficient to make the *N*-Sm*A* (very) weakly first. Although high-quality adiabatic scanning calorimetry (ASC)

*Electronic address: Jan.Thoen@Fys.kuleuven.ac.be

can determine minute latent heats, the first-order nature of the *N*-Sm*A* transition for wide nematic ranges (away from the tricritical point) could not be established in this way and the results were in agreement with the second-order de Gennes–McMillan result. Recently, however, Yethiraj and Bechhoefer [10], using a high-resolution real-space optical technique, presented quantitative evidence for the presence of a small two-phase region (of the order of 2 mK) and a smectic order parameter discontinuity for the *N*-Sm*A* transition of 8CB, considered to be of second order within experimental resolution in ASC experiments [11]. Derived values for the latent heats on the basis of the optical experiments [10] are, indeed, smaller than the resolution that had been obtained in the ASC experiments. These recent results confirm earlier work by Cladis *et al.* [12] and Anisimov *et al.* [13]. However, the presence of the very small discontinuities and small two-phase regions should have hardly an effect on the determination of the (effective) critical exponents, e.g., for the specific heat capacity or for the correlation lengths from x-ray scattering [3,7]. By far the dominant effect, introducing effective critical exponents near the (Landau) tricritical point, is the (de Gennes–McMillan) coupling between the nematic and smectic-*A* order parameters.

Since it is unlikely that one would find the proper conditions for a *N*-Sm*A* tricritical point in a pure compound (although 9CB is close [14]) measurements have usually been carried out in binary mixtures of liquid crystals (often of the same homologous series) to establish the proper width of the nematic range. It is then (implicitly) assumed that, as far as the *N*-Sm*A* transition is concerned, the mixture behaves as a pure compound and exponents relevant for the *N*-Sm*A* phase-transition behavior are obtained from the temperature dependence of the physical quantity considered at a given composition of the mixtures. This assumption is only valid as long as the *N*-Sm*A* transition temperature T_{NA} is only weakly dependent on the composition of the mixture. Fisher [15] has shown in 1968 that in mixtures the usual critical exponents are only obtained along a path of constant chemical potential difference and not along a path of constant composition x of the mixture, as is (necessarily) done experimentally. As long as dT_{NA}/dx is sufficiently small the usual exponents are obtained. In the other case one should observe exponent renormalization along paths of constant x.

Using a photopyroelectric ac calorimetric technique, we have investigated the phase-transition lines between the nematic and the smectic-*A* phase in two binary mixture systems showing so-called injected smectic-*A* phases. In both these systems, near the T_{NA} transition temperatures, the observed critical and tricritical specific heat capacity behavior is fully Fisher renormalized.

II. EXPERIMENTAL METHOD

The technique we used in this study of the specific heat capacity along phase-transition lines in the liquid crystal mixtures is in essence a low frequency operation of the inverse photopyroelectric setup we developed for the measurement of absolute values of the specific heat capacity and thermal conductivity of liquids [16] and gases [17]. Figure 1 gives a schematic diagram of the relevant parts of the applied one-dimensional geometry. The thin liquid crystal sample is put on top of a thin pyroelectric transducer. As a pyroelectric transducer we use a 75-μm-thick flat piece (15×15 mm^2) of $LiTaO_3$, which is gold coated on both sides. At the bottom, this pyroelectric transducer is illuminated with an intensity modulated laser beam. In this way the pyroelectric transducer acts as a temperature sensor as well as a heater (through the absorption of the modulated laser light by the gold coating). A detailed description of the practical implementation of the one-dimensional scheme can be found elsewhere [16].

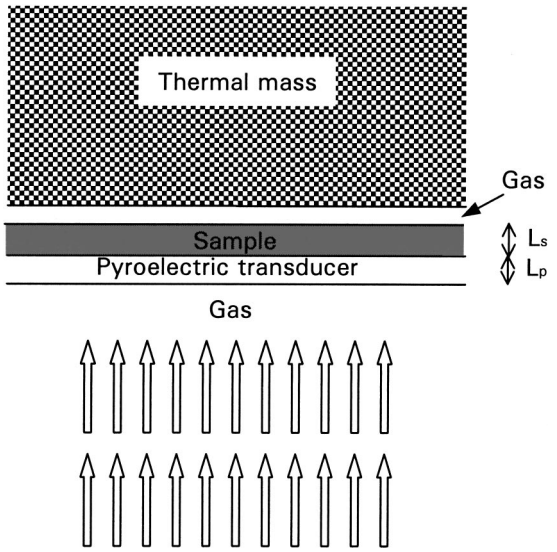

FIG. 1. Schematic representation of the one-dimensional photopyroelectric setup with the pyroelectric transducer, sample, thermal mass, and surrounding (inert) gas.

The light induced periodic heating gives rise to a temperature distribution $T(x,y,z,t)$ in the system, which is dependent on the modulation frequency, and on the geometry, and the thermal parameters of the assembly. The temperature variations in the pyroelectric transducer cause it to act as a current source, $i=pA[d\theta(t)/dt]$, which, considering the equivalent circuitry, results in a pyroelectric output voltage [18]

$$V(\omega)=H(\omega)pA\theta(\omega)e^{i\omega t}, \tag{1}$$

where p is the pyroelectric coefficient of the transducers, A is the transducer area, and $H(\omega)$ is an electrical transfer factor. $\theta(\omega)$ is the spatially averaged temperature variation in the detector with respect to the temperature T_0 of the measuring cell. In this inverse photopyroelectric (or front detection) geometry the signal output is determined by the distribution of the complex temperature of the different layers in the system. The resulting distribution is a complicated relation among the modulation frequency $f=\omega/2\pi$, the thickness L_s and L_p of sample and transducer, the width of the gas gap between sample and thermal load, and the thermal diffusivity α_j, and thermal effusivity e_j of the layers involved. The temperature $\theta_j(x)$ can be found, for the different layers, by solving the thermal diffusion equation for each layer [19]

$$\frac{\partial^2 \theta_j}{\partial x^2} = \frac{1}{\alpha_j}\frac{\partial \theta_j}{\partial t} - \frac{Q_j}{\kappa_j} \tag{2}$$

in which Q_j is the heat density in each layer, caused by the absorption of the modulated light, κ_j is the thermal conductivity of the layer considered. Because of the gold coating the pyroelectric transducer is opaque, and Q_j is nonzero only in the pyroelectric layer. The solutions of Eq. (2) are coupled by continuity conditions on temperature and heat flux at the interfaces and lead, in general, to complex expressions for the spatially averaged temperature $\theta(\omega)$ in the pyroelectric transducer [20,21,16].

At sufficiently low modulation frequencies one enters the so-called thermally very thin sample and detector regime, i.e., $L_s \ll \mu_s$ and $L_p \ll \mu_p$, with $\mu = (2\alpha/\omega)^{1/2}$ the thermal diffusion length. In this frequency range, the output voltage depends only on the heat capacity of the sample and of the pyroelectric transducer. In this regime the thermal conductivity κ, which normally is present in the equations via the diffusivity $\alpha = \kappa/\rho C_p$ (with ρ the density and C_p the specific heat capacity) and the effusivity $e = (\kappa \rho C_p)^{1/2}$, drops out of the equations, meaning that, in this frequency range, the thermal gradient over the detector and the sample are negligible and true calorimetric measurements can be performed. If one can further neglect the effusivity e_g of the surrounding gas compared to the effusivity of the sample e_s and of the detector e_p (e.g., for air or dry nitrogen e_g/e_s and e_g/e_p are smaller than 10^{-3}), the full expression of the one-dimensional model for sample and detector reduces to

$$\theta(\omega) = \frac{I_0}{4\pi i f}\frac{-1}{\rho_s C_s L_s + \rho_p C_p L_p}. \tag{3}$$

If desired, correction for the gas contributions (becoming more significant at very low frequencies) can be made in a straight-forward way [16]. Signals can be normalized with the (temperature dependent) bare pyroelectric signal. The normalized signal amplitude for the ac calorimetric mode is equal to

$$|V(\omega)|_{\text{norm}} = H(\omega)\frac{\rho_p C_p L_p}{\rho_s C_s L_s + \rho_p C_p L_p} \tag{4}$$

while the phase of the signal is constant. The sample independent parameters can, in principle, be obtained from calibration with known samples. From Eq. (3) or Eq. (4) one can see that in the ac calorimetric mode the parameters C_s and L_s are degenerate. In the full frequency range also the thermal conductivity κ_s appears as a third parameter in the degeneracy. This degeneracy can, however, as demonstrated in Ref. [16], be removed by measuring one, or more, frequency spectra with a thermal load (see Fig. 1) in the gas near the sample. This procedure also eliminates the need for calibration and one arrives at absolute values for C_p in the low frequency regime [16].

In our setup the pyroelectric transducer was illuminated with a 10-mW HeNe laser, modulated with an acousto-optic modulator. Only a fraction of the light energy is absorbed and for a beam diameter of about 6 mm, temperature oscillations (in the sample and detector) are estimated to be a few millikelvin. Amplitude and phase of the pyroelectric signal were recorded with a lock-in amplifier. The whole assembly was put in a temperature controlled oven, in which temperature control was achieved via a heating coil, a thermistor (near the sample), and a computer controlled servosystem.

III. EFFECTIVE EXPONENTS AND FISHER RENORMALIZATION

Modern theory of critical phenomena has resulted in the concepts of scaling and universality, leading to well-defined values of critical exponents for the power laws describing the fluctuation induced contributions of different physical quantities near the critical point. The excess heat capacity associated with fluctuations near a second-order transition $\Delta C_p = C_p - C_p^b$ (with C_p^b the background) can be represented by a simple power law expression or an expression including one or more correction-to-scale terms

$$\Delta C_p = A_0 t^{-\alpha}(1 + D_0 t^{\Delta} + \cdots) + B_0, \tag{5}$$

with $t = |(T - T_c)/T_c|$, α the relevant critical exponent, Δ the first correction-to-scaling exponent and A_0, B_0, D_0 system dependent nonuniversal parameters.

The N-SmA phase transition is expected to belong to the same universality class as the normal metal-to-superconductor transition, the lambda transition in helium and the three-dimensional XY model [5]. For this universality class of the XY-model values of $\alpha \approx -0.01$ and $\Delta \approx 0.5$ have been obtained [22–24]. Experimentally, however, in most cases positive α values are obtained [3,7], which implies that ΔC_p diverges at T_c instead of having a finite cusp value as implied from the (small) negative XY value. These positive (effective) exponents change with the width of the nematic range and are a consequence of the cross over between critical (XY) behavior and tricritical behavior with $\alpha = 0.5$. Indeed, the coupling between the smectic-A and the nematic order parameter results in first-order N-SmA transitions for narrow nematic ranges crossing over to second order at a tricritical point for wider nematic ranges [4–6].

The N-SmA transition has been studied in many cases in mixtures with a given composition as a function of the temperature. Calorimetric measurements result thus in values for C_{px}. However, isomorphism of critical phenomena requires that one should measure $C_{p\mu}$, as a function of t_μ, where μ designates a path of constant chemical potential difference [15,25]. For many mixtures, in particular, for mixtures of liquid crystal homologs, the distinction between C_{px} and $C_{p\mu}$ does not seem to be important and there are no apparent problems in analyzing the data with Eq. (5). In other cases, as in the systems studied here, the distinction between constant mole fraction x and constant chemical potential difference μ turns out to be important. Fisher [15] has shown that t_μ and t_x are related by

$$t_\mu(1 + \varepsilon') + \varepsilon t_\mu^{1-\alpha} = t_x(1 + \varepsilon''), \tag{6}$$

where $\varepsilon \approx (dT_c/dx)^2$ and ε' and ε'' are both small quantities proportional to ε. If ε is much smaller than 1 the distinction

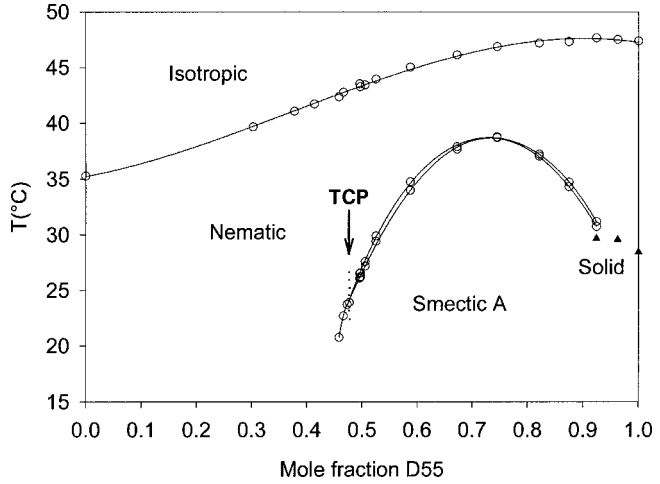

FIG. 2. Phase diagram of the binary system of 5CB and D55. Open circles indicate transition temperatures (and two-phase regions) obtained from the calorimetric measurements. The triangles indicate solidification points observed in cooling runs. TCP indicates the location of a tricritical point.

between μ and x is not important and no Fisher renormalization is obtained. If ε is sufficiently large there will be a region close to T_c where $t_\mu^{1-\alpha} \approx t_x$ since $t_\mu^{1-\alpha}$ goes to zero slower than t_μ. In this region one finds [26,27]

$$\Delta C_p^{\pm} = B - \frac{A^{\pm} t_x^{-\alpha_R}}{1 + D^{\pm} t_x^{-\alpha_R}}, \tag{7}$$

where the renormalized specific heat capacity exponent $\alpha_R < 0$ is defined by

$$\alpha_R \equiv -\alpha/(1-\alpha). \tag{8}$$

In Eq. (7) the superscript denotes above $(+)$ or below$(-)$ T_c, and B, $A^{\pm}$, and $D^{\pm}$ are adjustable parameters in a fit of the data. As already pointed out, whether Fisher renormalization is observed depends on the magnitude of dT_c/dx and also on the value of α [15,25]. Large values of $(dT_c/dx)^2$ and large positive values of α imply a large region of Fisher renormalization. Since for a tricritical point α is 0.5, positive and large, whether Fisher renormalization is observed, will depend mainly on the slope of the phase-transition line $T_{\mathrm{NA}}(x)$. A suitable parameter to characterize this dependence and compare different systems is

$$z \equiv \frac{1}{T_c^2}\left(\frac{dT_c}{dx}\right)^2. \tag{9}$$

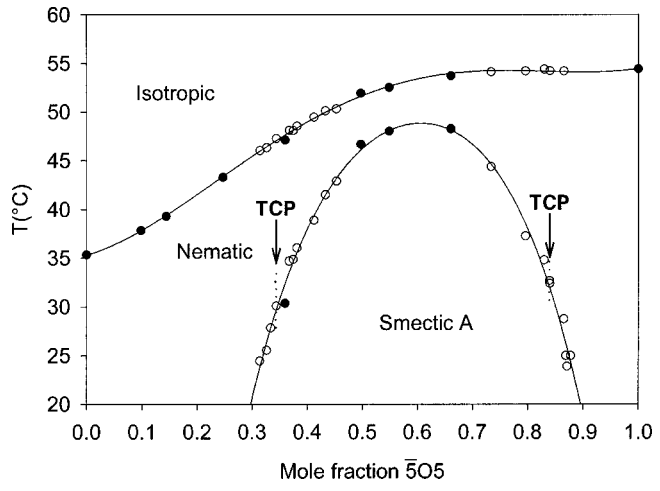

FIG. 3. Phase diagram of the binary system of 5CB and $\bar{5}$O5. Open circles are transition temperatures obtained from the calorimetric measurements. Solid dots are additional data obtained under a polarizing microscope. TCP indicates the location of a tricritical point.

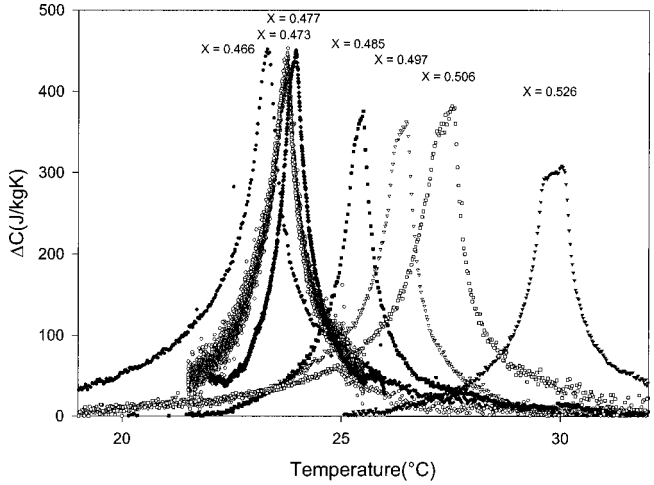

FIG. 4. Excess specific heat capacity for mixtures of 5CB and D55 near the tricritical point ($x \approx 0.47$).

IV. RESULTS AND DISCUSSION

We have carried out photopyroelectric ac calorimetry measurements by the method described in Sec. II along the

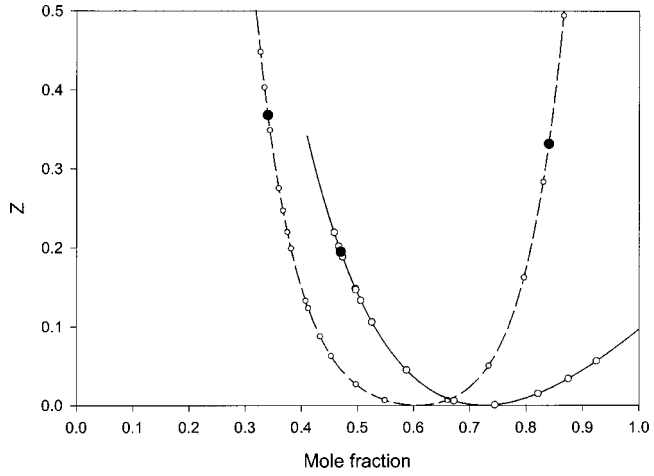

FIG. 5. Values of the parameter z of Eq. (9) as a function of mole fractions for the nematic–smectic-A transition lines. The open circles and the solid line give values for the binary system of 5CB+D55 as a function of the mole fraction of D55. Open circles and dashed line are for the binary system 5CB+$\bar{5}$O5 as a function of the mole fraction of $\bar{5}$O5. Solid dots indicate the value for the tricritical points in Figs. 2 and 3.

TABLE I. Results of least-squares fits of Eq. (7) to the excess specific heat capacity data near the tricritical point of the system 5CB+D55.

X_{D55}	T_c (K)	α_R	χ_ν^2
0.466	296.358±0.003	−0.96±0.06	1.09
0.473	298.436±0.003	−0.97±0.03	1.01
0.477	297.053±0.010	−1.03±0.05	1.36

N-Sm*A* transition line in two binary systems with so-called injected smectic-*A* phases, i.e., none of the pure compounds involved exhibit a smectic-*A* phase.

The first system we investigated is composed of 4-pentyl-4′-cyanobiphenyl (5CB) and 4-*n*-pentylphenyl-4′-*n*-pentylcyclohexyl-carboxylate (D55). The second was composed of 5CB and 4-*n*-pentyl 4′-*n*′ pentyloxybenzoate ($\overline{5}$O5). The compounds 5CB and D55 were obtained from Merck (Germany) and $\overline{5}$O5 from AWAT Co Ltd (Poland). The phase diagram of the 5CB+*D*55 system is shown in Fig. 2. The open circles are transition temperatures derived from the calorimetric measurements. The smectic-*A* range shows a domelike structure with a rather strong concentration dependence of the *N*-Sm*A* transition temperature on either side of the top. At the top, the nematic range is rather small, and according to the theoretical expectations [4–6] the transitions near the top are expected to be of first order. Although (photopyroelectric) ac calorimetry cannot measure latent heats and unambiguously establish the first-order nature of the transition, the presence of a first-order transition manifests itself by anomalous changes in the photopyroelectric signal phase, which is almost zero for continuous transitions. The width of the two-phase regions of first-order transitions can also be well determined by slope discontinuities in the amplitude and phase signals. In Fig. 2 the width of the two-phase region is, where sufficiently wide, indicated by two symbols for the mole fraction considered. The NI transition is also first order everywhere but the width of the two-phase region is too small to be visible in Fig. 2. In Fig. 2 it can also be observed that the width of the two-phase region becomes apparently zero at the top. This is consistent with thermodynamics arguments [28,29]. If, at the top, the two-phase region were not zero the mixture would have split in two nematic phases with different composition, for which there is no indication. The transitions at the top remain, however, clearly first order as could be clearly observed in the signal phase and also confirmed in an adiabatic scanning calorimetric (ASC) experiment [30]. ASC allows the measurement of the enthalpy as a function of the temperature

TABLE II. Results of least-squares fits of Eq. (5) to the excess specific heat capacity data near the tricritical point of the system 5CB+D55.

X_{D55}	T_c (K)	α	χ_ν^2
0.466	296.363±0.004	0.26±0.02	4.29
0.473	298.383±0.001	0.013±0.010	6.06

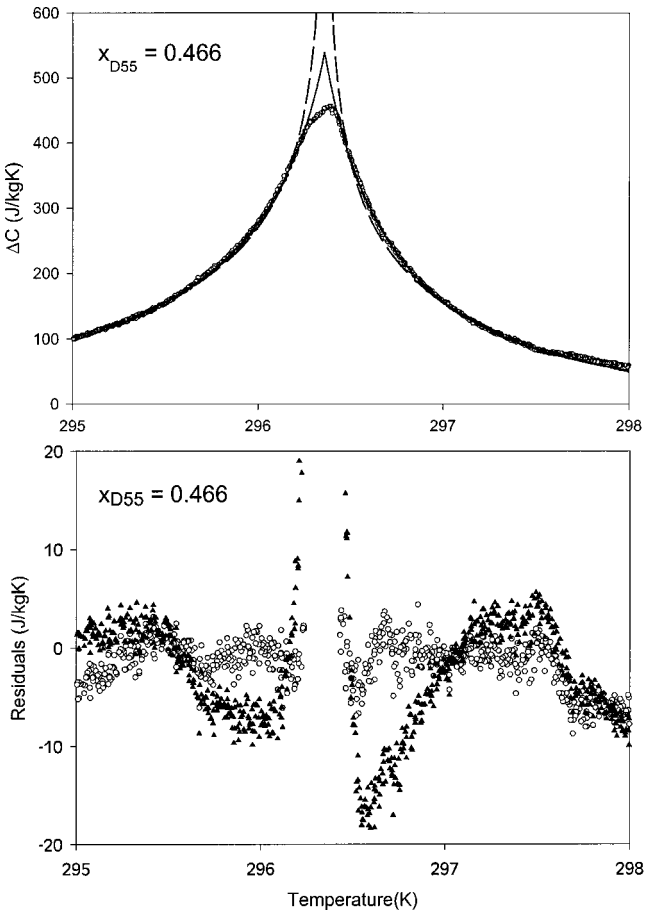

FIG. 6. The upper part gives a comparison of fits with Eq. (5) (dashed line) and Eq. (7) (solid line) to the ΔC data at $x_{D55}=0.466$ near the tricritical point along the nematic–smectic-*A* transition line in the binary system 5CB+D55. The lower part gives the corresponding residuals. Solid triangles are for the fit with Eq. (5) and open circles for the fit with Eq. (7).

[1,3] and permits one to deduce latent heat values at first-order transitions. For a mole fraction 0.722 of D55 (very near the top) an almost vertical step in the enthalpy curve was observed, resulting in a latent heat value of 2800 J/kg. For wider nematic ranges on the low mole fraction side of the top, the two-phase region becomes narrower and narrower and disappears at a tricritical point (to be discussed further) with a mole fraction of about 0.47. On the right hand side of the top, the width of the nematic phase also increases and one would expect here also a tricritical point. This point could, however, not be located because in this range the mixtures solidified (at temperatures indicated by triangles in Fig. 2) before the *N*-Sm*A* transition could be reached.

The phase diagram of the second binary system 5CB and $\overline{5}$O5 is given in Fig. 3. The open symbols are transition temperatures from the pyroelectric ac calorimetric measurements, the solid ones have been determined with a polarizing microscope. Both methods give consistent results. The phase diagram for this system determined earlier by Dunmur, Walker, and Palfly-Muhoray [31] is only in qualitative agreement with our present results. These authors found quite wide (several degrees) two-phase regions for parts of the

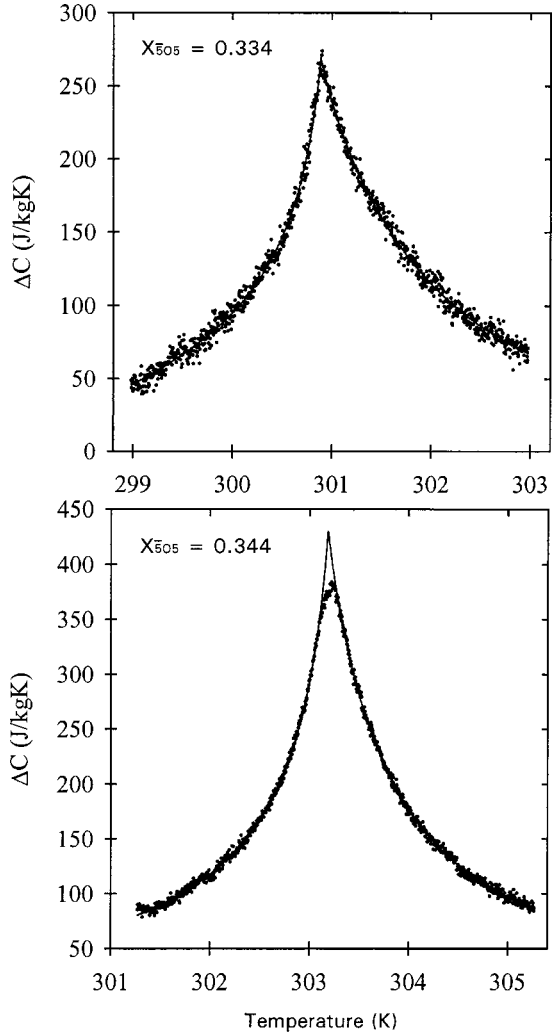

FIG. 7. Fits with Eq. (7) to data for two mole fractions near the lower $x_{\bar{5}O5}$ mole fraction tricritical point (see Fig. 3) in the binary system 5CB+$\bar{5}$O5.

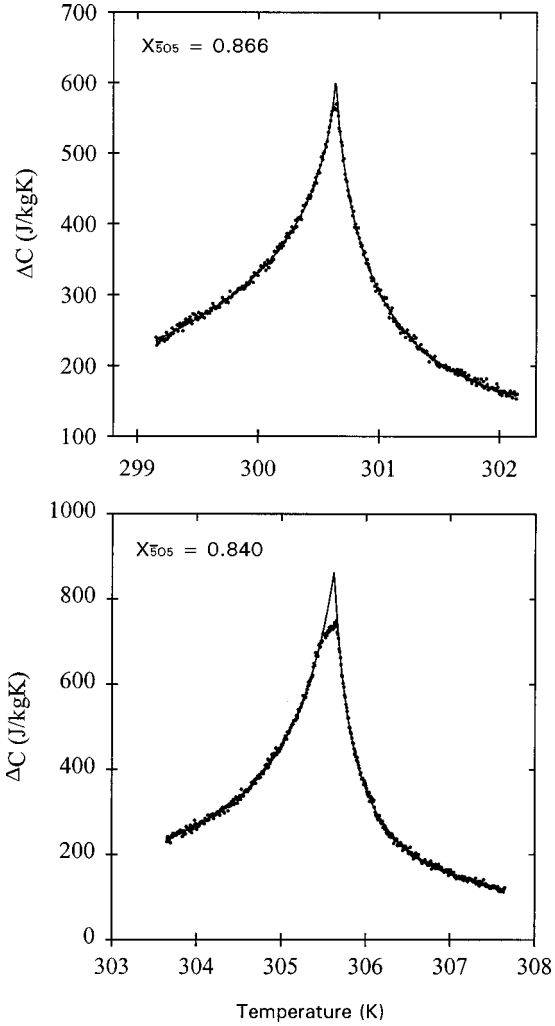

FIG. 8. Fits with Eq. (7) to data for two mole fractions near the upper $x_{\bar{5}O5}$ mole fraction tricritical point (see Fig. 3) in the binary system 5CB+$\bar{5}$O5.

N-Sm*A* transition line, also at the top of the dome, which is, as already pointed out, on thermodynamic grounds not to be expected. In this system, which has a more symmetric *N*-Sm*A* transition line, we did not encounter solidification problems and a tricritical point (TCP) could indeed, be located on either side of the Sm*A* dome.

In Fig. 4 the specific heat capacity behavior for mole fractions near the TCP of 5CB and D55 are given. The tricritical point occurs in a mixture around $x=0.47$. For higher concentrations one clearly observes the width of the two-phase region. Instead of a large diverging anomaly, one clearly observes a cusplike behavior. A similar behavior has also been observed by Huster, Stine, and Garland [26] for the *N*-Sm*A* tricritical region of $\bar{7}$S5 and 8OCB and by Stine and Garland [27] for 8OCB and TBBA. In both cases a large value for the parameter z of Eq. (9) was found ($z_{\mathrm{TCP}}=0.74$ and $z_{\mathrm{TCP}}=0.43$, respectively) and the tricritical exponent α was fully renormalized. In Fig. 5 the values of the parameter z are given along the *N*-Sm*A* transition lines of 5CB and D55 and of 5CB and $\bar{5}$O5. For the former system a value $z_{\mathrm{TCP}}=0.20$ is found for the tricritical mole fraction of 0.47. This is also a quite large value and would infer substantial Fisher renormalization. We have carried out fits for different ranges of the data with the unrenormalized power law expression of Eq. (5) and the renormalized form given in Eq. (7) for three concentrations ($x=0.466$, 0.473 and 0.477) near the tricritical one. Only with Eq. (7) could good fits be obtained indicating full Fisher renormalization of the tricritical $\alpha=0.5$ value. Fit results are given in Tables I and II. In Fig. 6 fits with a normal power law and with the renormalized expression are compared for $x_{\mathrm{D55}}=0.466$.

For the second system investigated 5CB and $\bar{5}$O5 two tricritical points are found, one on either side of the smectic-*A* dome in Fig. 3, for the mole fraction $x_{\bar{5}O5}=0.34$ and $x_{\bar{5}O5}=0.84$. Our location of the tricritical point on the low $x_{\bar{5}O5}$ side of the dome coincides within experimental uncertainty with the location obtained by Cross and Fung [32] on the basis of a NMR investigation. On the basis of the z curve in Fig. 5 for this system, one finds again large values ($z_{\mathrm{TCP}}=0.37$ and $z_{\mathrm{TCP}}=0.33$, respectively). Thus cusplike C_p peaks and substantial Fisher renormalization are to be ex-

TABLE III. Results of least-squares fits of Eq. (7) to the excess specific heat capacity data near the low $\overline{5}$O5 mole fraction tricritical point of the system 5CB+$\overline{5}$O5

$x_{\overline{5}O5}$	T_c (K)	α_R	χ^2_ν
0.314	297.530±0.058	−0.88±0.15	1.68
0.326	298.672±0.010	−0.85±0.14	1.57
0.334	300.873±0.025	−0.88±0.08	1.09
0.344	303.193±0.047	−0.96±0.06	1.13

TABLE IV. Results of least-squares fits of Eq. (7) to the excess specific heat capacity data near the upper $\overline{5}$O5 mole fraction tricritical point of the system 5CB+$\overline{5}$O5.

$x_{\overline{5}O5}$	T_c (K)	α_R	χ^2_ν
0.871	297.07±0.03	−0.540±0.088	2.56
0.866	300.64±0.02	−0.764±0.036	1.06
0.840	305.62±0.03	−0.991±0.016	1.18

pected. This is indeed found for the results given in Fig. 7 for the mole fractions $x_{\overline{5}O5}=0.334$ and $x_{\overline{5}O5}=0.344$ and in Fig. 8 for the mole fractions $x_{\overline{5}O5}=0.840$ and 0.866. Here also good fits could be obtained with the renormalized expression of Eq. (7). In Table III fitting parameter results are given for the first tricritical point ($x_{\overline{5}O5}=0.34$) region and for some lower mole fractions. In Table IV analogous results are given for the second tricritical point ($x_{\overline{5}O5}=0.84$) and for some larger mole fraction. On both sides of the dome, for larger nematic ranges away from the tricritical points, full renormalization still occurs but, as expected, lower corresponding unrenormalized effective exponents are obtained.

ACKNOWLEDGMENTS

This work was financially supported by the Fund for Scientific Research Flanders (Belgium) (FWO, Project No. G.0264.97).

[1] J. Thoen, in *Phase Transitions in Liquid Crystals*, Vol. 290 of *NATO Advanced Studies Institute, Series B: Physics*, edited by S. Martellucci and A. N. Chester (Plenum, New York, 1992), pp. 155–174.
[2] C. W. Garland, in *Phase Transitions in Liquid Crystals* (Ref. [1]), pp. 175–187.
[3] J. Thoen, Int. J. Mod. Phys. B **9**, 2157 (1995); in *Liquid Crystals in the Nineties and Beyond*, edited by S. Kumar (World Scientific, Singapore, 1995), Chap. 2, p. 19; in *Physical Properties of Liquid Crystals*, edited by D. Demus, J. Goodby, G. W. Gray, H. W. Spiess, and V. Vill (Wiley-VCH, Weinheim, 1997), pp. 208–232.
[4] P. G. de Gennes, Solid State Commun. **10**, 753 (1972).
[5] P. G. de Gennes and J. Prost, *The Physics of Liquid Crystals*, 2nd ed. (Clarendon, Oxford, 1993).
[6] W. L. McMillan, Phys. Rev. A **6**, 936 (1972).
[7] C. W. Garland and G. Nounesis, Phys. Rev. E **49**, 2964 (1994), and references therein.
[8] J. Als-Nielsen, J. D. Litster, R. J. Birgeneau, M. Kaplan, C. R. Safinya, A. Lindegaard-Andersen, and S. Mathiesen, Phys. Rev. B **22**, 312 (1980).
[9] B. I. Halperin, T. C. Lubensky, and S. K. Ma, Phys. Rev. Lett. **32**, 292 (1974).
[10] A. Yethiraj and J. Bechhoefer, Phys. Rev. Lett. **84**, 3642 (2000).
[11] J. Thoen, A. Marijnissen, and W. Van Dael, Phys. Rev. A **26**, 2886 (1982).
[12] P. E. Cladis, W. van Saarloos, D. A. Huse, J. S. Patel, J. W. Goodby, and P. L. Finn, Phys. Rev. Lett. **62**, 1764 (1989).
[13] M. A. Anisimov, P. E. Cladis, E. E. Gorodetskii, D. A. Huse, V. E. Podneks, V. G. Taratuta, W. van Saarloos, and V. P. Voronov, Phys. Rev. A **41**, 6749 (1990).
[14] J. Thoen, H. Marijnissen, and W. Van Dael, Phys. Rev. Lett. **52**, 204 (1984).
[15] M. E. Fisher, Phys. Rev. **176**, 257 (1968).
[16] J. Caerels, C. Glorieux, and J. Thoen, Rev. Sci. Instrum. **69**, 2452 (1998).
[17] J. Caerels, C. Glorieux, and J. Thoen, Rev. Sci. Instrum. **71**, 3506 (2000).
[18] H. J. Coufal, R. K. Grygier, D. E. Horne, and J. E. Fromm, J. Vac. Sci. Technol. A **5**, 2875 (1987).
[19] A. Mandelis and M. M. Zver, J. Appl. Phys. **57**, 4421 (1985).
[20] D. Darladat, M. Chirtoc, C. Nematu, C. M. Candea, and D. Bicanic, Phys. Status Solidi A **121**, K231 (1990).
[21] M. Chirtoc and G. Michailescu, Phys. Rev. B **40**, 9606 (1989).
[22] C. Bagnuls and C. Bervillier, Phys. Rev. B **32**, 7209 (1985).
[23] C. Bagnuls and C. Bervillier, D. I. Meiron, and B. G. Nickel, Phys. Rev. B **35**, 3585 (1987).
[24] R. Guida and J. Zinn-Justin, J. Phys. A **31**, 8103 (1998).
[25] M. A. Anisimov, A. V. Voronel, and E. E. Gorodeskii, Sov. Phys. JETP **33**, 605 (1971).
[26] M. E. Huster, K. J. Stine, and C. W. Garland, Phys. Rev. A **36**, 2364 (1987).
[27] K. J. Stine and C. W. Garland, Phys. Rev. A **39**, 1482 (1989).
[28] J. N. Murrel and E. A. Boucher, *Properties of Liquids and Solutions* (Wiley, York, 1982).
[29] H. A. Oonk, *Phase Theory: The Thermodynamics of Heterogeneous Equilibria* (Elsevier Scientific, Amsterdam, 1981).
[30] L. Van Genechten, Lic. Thesis, K. U. Leuven, 1999.
[31] D. A. Dunmur, R. G. Walker, and P. Palfly-Muhoray, Mol. Cryst. Liq. Cryst. **122**, 321 (1985).
[32] C. W. Cross and B. M. Fung, Liq. Cryst. **19**, 863 (1995).